ALSs with Conventional and Fuzzy Controllers Considering Wind Shears and Gyro Errors

Romulus Lungu[1], Mihai Lungu[2], and Lucian T. Grigorie[3]

University of Craiova, Romania, Code: 200440

The paper presents the automatic control of the aircrafts in the longitudinal plane during the landing process, taking into account the wind shears and sensor errors. Two automatic landing systems (ALS) are designed: the former uses an Instrumental Landing System (ILS), while the latter controls the flight altitude using the state vector. Both systems have a subsystem for the control of longitudinal velocity, which is based on the dynamic inversion theory. The subsystems for the pitch angle control use proportional-derivative control laws or a law based on the dynamic inversion theory and a proportional-integral-derivative controller. The slope and flare controllers are a proportional-derivative (PD) controller and a proportional-integral-derivative (PID) controller, respectively. The controllers are designed both in classical and fuzzy logic approaches. Theoretical results are validated by numerical simulations in the absence or presence of wind shears and sensor errors. The analysis of the main ALS parameter time evolutions leads to conclusions regarding the superiority of the dynamic qualities for the ALS with fuzzy controllers**.**

Subject headings: Control systems, Fuzzy sets, Aircraft, Wind gusts, Sensors.

Notation

$\mathbf{A}, \mathbf{B}$	=	matrices in the state equation
A, B	=	fuzzy sets in the antecedent (fuzzy systems)
$\overline{A_0 A_\infty}$	=	flare curve of the landing process
A_q^i	=	associated individual antecedent fuzzy sets of each input variable (fuzzy systems)
$\overline{A_p A_0}$	=	aircraft trajectory for the first landing phase
a_k^i	=	parameters of the linear function (fuzzy systems)
a_r	=	acceleration applied along an arbitrary direction
$\overline{B}$	=	sensor bias
b_0^i	=	scalar offset (fuzzy systems)
d	=	aircraft deviation in vertical plane with respect to the glide slope (GS)
e	=	operating error of the fuzzy systems

[1] Professor PhD, University of Craiova, Avionics Division, Decebal Blv., no.107, E-mail: romulus_lungu@yahoo.com
[2] Lecturer PhD, University of Craiova, Avionics Division, Decebal Blv., no.107, E-mail: Lma1312@yahoo.com
[3] Assistant Professor PhD, University of Craiova, Avionics Division, Decebal Blv., no.107, E-mail: ltgrigorie@yahoo.com

f = polynomial function (fuzzy systems)

H = aircraft altitude

H_0 = starting altitude for the flare phase of the landing process

H_{ref} = reference altitude

H_c = imposed altitude for each point of the glide slope

H_p = altitude at which the landing process starts

$i(t)$ = command variable in time (fuzzy systems)

K = scale factor of the sensor

k_p, k_d = proportional gain and derivative gain (fuzzy systems), respectively

k_p^h = proportional component of the reference angle control law θ_r

k_{pi}^h = integral component of the reference angle control law θ_r

k_{pd}^h = derivative component of the reference angle control law θ_r

$k_p^{\theta}, k_p^{\dot{\theta}}$ = gains of the angle gyro and of the angular rate gyro, respectively

m_c = calculated values of the variables m

N = number of rules (fuzzy systems)

R = distance from the aircraft to the intersection point between the Runway and glide slope (GS)

S = sensor sensibility to the acceleration a_r applied along an arbitrary direction

s = cosine function (fuzzy systems)

T_0 = flight time for the wind shear

T_S = sample period (fuzzy systems)

t_0 = starting time moment of the flare phase

t_d = time moment when the aircraft touches the runway

$\mathbf{u}$ = command vector in the state equation

V_0 = nominal velocity of the aircraft.

V_{vx} = longitudinal component of the wind velocity

V_{vz} = vertical component of the wind velocity

V_x = aircraft velocity along the axis Ox (longitudinal axis of the aircraft)

V_{x_c} = desired velocity along the longitudinal aircraft axis

$\overline{V}_x, \dot{\overline{V}}_x$ = outputs of the first order command filter

v = noise of the sensor

$\mathbf{v}_{\mathbf{v}}$ = vector of disturbances (it contains the components of the wind velocity along aircraft axes Ox and Oz)

$w^i(\boldsymbol{x})$ = degree of fulfillment of the antecedent (the level of firing of the i^{th} rule in fuzzy systems)

x = aircraft horizontal displacement

$\mathbf{x}$ = state vector

$\dot{x}$ = aircraft horizontal velocity

$\bar{\boldsymbol{x}}$ = input vector (fuzzy systems)

$\bar{x}$ = independent variable on the universe (fuzzy systems)

$\bar{x}_{left}$ = left breakpoint (fuzzy systems)

$\bar{x}_q$ = individual input variables

$\bar{x}_{right}$ = right breakpoint

y = crisp function in the consequent (fuzzy systems)

y^i = first order polynomial function in the consequent (fuzzy systems)

z, π = fuzzy functions

α = attack angle of the aircraft

δ_p = aircraft elevator deflection

δ_T = command of the aircraft engine

Δe = change in error (fuzzy systems)

ΔK = calibration error of the sensor scale factor

Γ = aircraft angular deviation

γ = aircraft flight path angle

γ_c = imposed glide slope of the aircraft

ω = output angular rate (the perturbed signal)

ω_i = angular rate (input of the error model)

ω_y = pitch angular rate of the aircraft

τ = time constant of the aircraft movement (glide slope phase)

θ = aircraft pitch angle

θ_c = calculated pitch angle of the aircraft

θ_r = pitch reference angle of the aircraft

$\bar{\theta}$ = input of the command filter

$\dot{\bar{\theta}}$ = input of the command filter

$\ddot{\bar{\theta}}$ = input of the command filter

$\dot{\theta}, \dot{\psi}$ = aircraft angular rates

$\ddot{\theta}_c$ = calculated pitch angular acceleration of the aircraft

I. Introduction

The first Automatic Landing System (ALS) was designed in England in 1965. From that moment, most aircrafts have ALS based on the Instrumental Landing System (ILS) for the aircrafts control (Donald 1990; Aron et al. 1989), which use proportional-derivative (PD), proportional-integral (PI) or proportional-integral-derivative (PID) conventional laws for the altitude and descend velocity control (Singh and Padhi 2008; Juang and Cheng 2006; Lungu 2008), and PD or PID conventional laws for the pitch angle and pitch rate control. These control laws use the state vector or the dynamic inversion concept and they have a command filter, dynamic compensators, and state observers (Lungu 2008; Che and Chen 2001; Kang and Isidori 1992; Kawaguchi et al. 2008; Calise and Rysdyk 1999; Pashilkar et al. 2006; Lungu 2000).

The use of GPS and the performance increase of the sensors for the angular variables measurement lead to the increase of the landing trajectory track accuracy (Lungu 1997; Aron and Lungu 1994; Lungu and Grigorie 2005; Grigorie 2007). The sensor errors must have an insignificant influence on the landing process performances.

For different flight conditions, the controlled parameters should be kept in a specific flight envelope, defined by the Federal Aviation Administration (FAA). The environment conditions required by FAA are: head wind – 25 knots, rear wind – 10 knots, lateral wind – 15 knots, moderate turbulence, wind shears of 8 knots per 100 ft at 200 ft to touchdown (Che and Chen 2001; FAA 1971; Niewoenhner and Kaminer 1996). If the flight conditions are outside the specific envelope, then the ALS is disabled, and the pilot takes the aircraft control. It is possible that a non-experienced pilot does not succeed in controlling the aircraft during the landing process. According to the international statistics, 62% of aircraft accidents are due to the atmospheric disturbances (wind disturbances).

In recent years lots of scientific researches have applied the intelligent concepts for the aircrafts automatic control during the landing process; they use the optimal synthesis $H_2, H_\infty, H_2 / H_\infty$ and the adaptive synthesis based on the dynamic inversion theory (Che and Chen 2001; Niewoenhner and Kaminer 1996; Liao et al. 2005), the neural networks theory (Singh and Padhi 2008; Mori and Suzuki 2009; Niculescu 2001; MIT Open Course 2007; Kargin 2007; Vo and Sridhar 2008), or fuzzy techniques (Abdullah and Ayman 2008; Zdenko and Stjepan 2006; Verbruggen and Bruijn 1997; Hampel et al. 2000; Zadeh 1965; Tomescu 2001; Jantzen 1998; Kumar et al. 2008; Mahfouf et al. 1999). These intelligent techniques have the advantage of very good adaptability, robustness, and software implementation capabilities.

This paper approaches the automatic control of aircrafts in the longitudinal plane during the landing process, taking into consideration the longitudinal and vertical wind shears and the errors of the sensors. Two automatic landing systems (ALS) are designed: the former uses an ILS system, while the latter controls the altitude using the state vector. Both systems have a subsystem for the control of the longitudinal velocity V_x; the velocity control uses the dynamic inversion and a first order command (reference) filter.

The ALS with ILS system has a proportional-derivative pitch angle control system, and uses some sensors for the pitch angular rate and pitch angle measurement; the sensor for the measurement of the pitch angle may miss if the pitch angle signal is obtained by numerical integration of the angular rate ω_y. The second ALS has a pitch angle control system based on the dynamic inversion, PID controller, and a second order command filter.

The paper has a lot of original issues; some of them are: the general design of the two new ALSs including the longitudinal velocity control, the tuning of the PID conventional controllers for the altitude, pitch and velocity channels, the design of the above controllers in an intelligent approach by using the fuzzy techniques, the study of the errors induced by the wind shears and errors of the gyro sensors on the both variants of the ALS (with conventional and fuzzy control). In section VII of the paper, all the originality issues are presented in detail.

The paper is organized as follows: the geometry of the landing process, in longitudinal plane, is given in section II, the dynamics of the aircraft in longitudinal plane is presented in section III; in section IV the authors present the two new automatic landing systems for aircrafts flight control in longitudinal plane. The design of the fuzzy logic controllers is given in section V, while, in section VI, complex simulations have been performed to validate the proposed automatic landing systems; finally, some conclusions are shared in section VII.

II. Geometry of the Landing Process in Longitudinal Plane

If only the longitudinal plane approach is considered for the landing of an aircraft, then two phases are distinguished for this procedure (Fig. 1): 1) Glide slope (GS) phase ($H \geq H_0$), and 2) Flare phase ($H < H_0$); H is the aircraft altitude and H_0 is the starting altitude for the flare landing phase.

In the glide slope phase of the landing process, an Instrumental Landing System (ILS) may be used to elaborate the signals for the aircraft flight control. In this way, the slope receiver forms a signal which depends on the angular deviation Γ (Fig. 1) provided by ILS; it is a guidance signal for the control system of the aircraft pitch angle (Donald 1990). A low-pass filter is used to cut the noise generated by the distortions from the equal signals zone (Aron et al. 1989). The control loop of the guidance system is closed by the aircraft kinematics, which transforms the aircraft pitch in a displacement with respect to the imposed (desired) glide slope γ_c. Usually, the value of the desired glide slope γ_c is $-2.5\deg$. The other variables in Fig. 1 are: $\gamma-$ flight path angle; $d-$ the aircraft deviation in vertical plane with respect to GS, $R-$ the distance from the aircraft to the intersection point between the Runway and GS, and $V_0 -$ the nominal velocity of the aircraft.

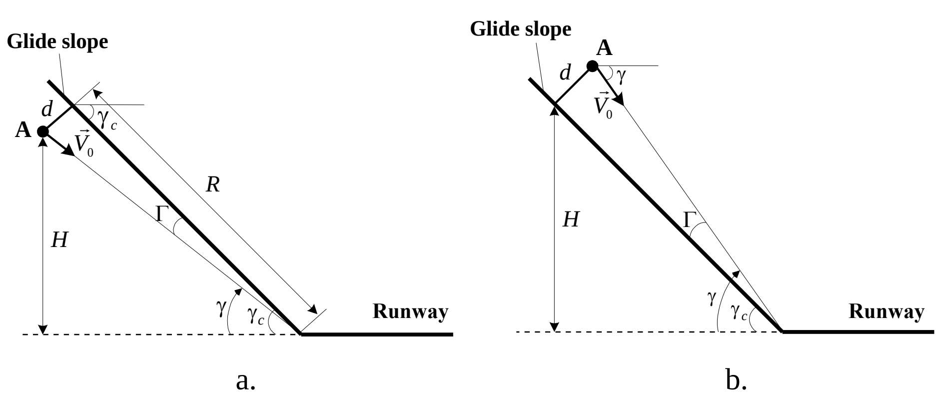

Fig. 1 The movement geometry during the glide slope landing phase

The angular deviation Γ is expressed by one of the following formulas:

$$\Gamma = \frac{d}{R}[\text{rad}], \Gamma = 57.3\frac{d}{R}[\text{deg}]. \tag{1}$$

while the component of the aircraft velocity along the normal direction to the glide slope is given by the equation:

$$\dot{d} = V_0 \sin\Gamma \cong \frac{V_0}{57.3}\Gamma, [\Gamma] = \text{deg}. \tag{2}$$

For the two landing cases presented in Fig. 1, the relations between the angular variables can be expressed as follows:

$$\gamma_c = |\Gamma| + \gamma, \gamma = |\Gamma| + \gamma_c; \tag{3}$$

γ, γ_c, and Γ are expressed here in degrees.

In the second landing phase (flare phase), the aircraft altitude may be expressed by using the equation:

$$\tau\dot{H} + H = 0, \tag{4}$$

where τ is the time costant of the aircraft movement (glide slope phase).

According to Fig. 2, the descendent rate, in the moment of the flare maneuver starting, is:

$$\dot{H}_0 = V_0 \sin\gamma_c = V_0 \sin(-2.5\,\text{deg}) \cong \frac{-2.5}{57.3}V_0, \tag{5}$$

while, during the flare process, according to equation (4), it becomes:

$$\dot{H} = -\frac{H}{\tau}. \tag{6}$$

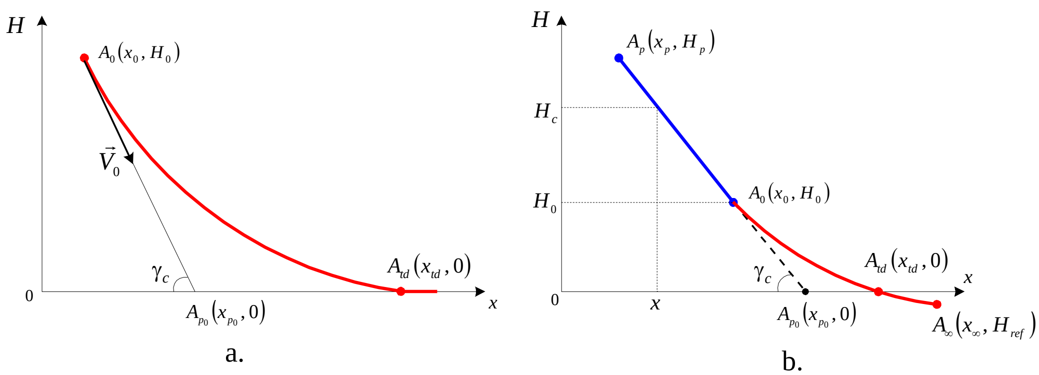

Fig. 2 The movement geometry during the flare landing phase

If the flare process takes, for example, 5τ seconds (Donald 1990), and the velocity of the aircraft has not a significant variation, then, from Fig. 2.a, the coordinates of the contact point between the aircraft and the runway are:

$$x_{td} - x_0 = V_0 \cdot 5\tau . \tag{7}$$

Using the equation (6) for $H = H_0$ and the equation (5), we obtain:

$$H_0 = \frac{2.5}{57.3} V_0 \tau , \tag{8}$$

and, from Fig. 2.a, we get:

$$H_0 = -\left(x_{p_0} - x_0\right)\tan\gamma_c = 0.0435 \cdot \left(x_{p_0} - x_0\right). \tag{9}$$

The equations (8) and (9) lead to the following one:

$$V_0 \tau = c_1 \cdot \left(x_{p_0} - x_0\right), \tag{10}$$

where $c_1 = \left(\frac{57.3}{2.5} \cdot 0.0425\right) = 0.9741$. If the values of V_0 and H_0 are known, using the equations (7) and (10), we successively obtain the values of τ, x_{p_0}, and x_{td};

$$x_{td} = x_0 + c_2 H_0 , \tag{11}$$

with $c_2 = 5c_1 / 0.0435 \cong 112$.

For this landing phase, a radio-altimeter is used to provide the altitude signal for the aircraft flight control. The input signal of the controller for the flare curve, depending on $\dot{H}$ (with $\dot{H}$ of the form in (6)), may be determined by using the equation of the aircraft kinematics, i.e.:

$$\dot{H} = V_0 \gamma, \gamma = \theta - \alpha ; \tag{12}$$

θ is the aircraft pitch angle, $\alpha -$ the attack angle of the aircraft, while γ is the aircraft flight path angle (θ, α, and γ are expressed here in radians).

Because the flare trajectory is an exponential one, the aircraft would take a very long time to reach the point A_{td}. For this reason, the altitude H_{ref} is chosen to be negative (see Fig. 2.b, where $\overline{A_p A_0}$ is the aircraft trajectory for the first landing phase, while $\overline{A_0 A_\infty}$ is the flare curve). The coordinate x_{p_0} is expressed from the equation of the segment $\overline{A_p A_{p_0}}$. Thus,

$$x_{p_0} = x_p + \frac{H_p}{\tan\gamma_c} . \tag{13}$$

The imposed altitude H_c for each point of the glide slope is calculated with the formula:

$$H_c = H_p + \left(x_p - x\right)\tan\gamma_c , \tag{14}$$

while, for the flare curve, the next equation can be used (Singh and Padhi 2008):

$$H_c = H_{ref} + \left(H_0 - H_{ref}\right) \cdot \exp\left[-k_x\left(x - x_0\right)\right]. \tag{15}$$

If H_0 and x_0 are known, the unknown variables H_{ref} and k_x may be calculated. Other equations for the calculus of the flare trajectory parameters are, for example, the ones in (Juang and Cheng 2006), i.e.:

$$H_c = H_0 \exp\left(-\frac{t - t_0}{\tau}\right), H_0 = H_c\left(t_0\right), \tau = -\frac{H_0 V_G}{\dot{H}_0 - \dot{H}_{td}}, \dot{H}_0 = \dot{H}_c\left(t_0\right), \dot{H}_{td} = \dot{H}_c\left(t_d\right). \tag{16}$$

t_0 is the starting time moment of the flare phase, while t_d $-$ the time moment when the aircraft touches the runway;

$$V_G = V_0 \cos\gamma + V_{vx}, \tag{17}$$

with V_{vx} $-$ the horizontal velocity of the wind. With $t - t_0 = \left(x - x_0\right) / \dot{x}$, the equation (16) gets the form:

$$H_c = H_0 \exp\left(-\frac{x - x_0}{\tau \dot{x}}\right). \tag{18}$$

As a consequence, the equations (13) and (14) are used for the H_c calculus during the glide slope landing phase $\left(H \geq H_0\right)$, while the equations (10) and (18) are used for the H_c calculus during the second landing phase $\left(H < H_0\right)$; x and $\dot{x}$ are the aircraft horizontal displacement and the aircraft horizontal velocity, respectively;

$$\dot{x} = V_x \cos\theta + V_z \sin\theta = V_x \cos\theta + V_0 \sin\alpha \sin\theta. \tag{19}$$

III. The Dynamics of the Aircraft in Longitudinal Plane

The linear model of the aircraft movement, in longitudinal plane, is described by the state equation:

$$\dot{\mathbf{x}} = \mathbf{A}\mathbf{x} + \mathbf{B}\mathbf{u} + \mathbf{B_v}\mathbf{v_v}, \tag{20}$$

with $\mathbf{x}$ - the state vector, $\mathbf{u}$ $-$ the command vector, $\mathbf{v_v}$ $-$ the vector of disturbances (it contains the components of the wind velocity along aircraft axes Ox and Oz),

$$\mathbf{x} = \left[V_x \;\; \alpha \;\; \omega_y \;\; \theta\right]^T, \mathbf{u} = \left[\delta_p \;\; \delta_T\right]^T, \mathbf{v_v} = \left[V_{vx} \;\; V_{vz}\right]^T, \tag{21}$$

$$\mathbf{A} = \begin{bmatrix} a_{11} & a_{12} & a_{13} & a_{14} \\ a_{21} & a_{22} & a_{23} & a_{24} \\ a_{31} & a_{32} & a_{33} & a_{34} \\ 0 & 0 & 1 & 0 \end{bmatrix} = \begin{bmatrix} X_u & X_w & 0 & -g\cos\theta_0 \\ Z_u^* & Z_w & 1 & -\left(g / V_0\right)\sin\theta_0 \\ \tilde{N}_u & \tilde{N}_w & \tilde{N}_q & \tilde{N}_\theta \\ 0 & 0 & 1 & 0 \end{bmatrix}, \mathbf{B} = \begin{bmatrix} b_{11} & b_{21} & b_{31} & 0 \\ b_{12} & b_{22} & b_{32} & 0 \end{bmatrix}^T = \begin{bmatrix} 0 & Z_{\delta_p} / V_0 & \tilde{N}_{\delta_p} & 0 \\ X_{\delta_T} & Z_{\delta_T} / V_0 & N_{\delta_T} & 0 \end{bmatrix}^T, \tag{22}$$

$$\mathbf{B_v} = \begin{bmatrix} -a_{11} & -a_{21} & -a_{31} & 0 \\ -a'_{12} & -a'_{22} & -a'_{32} & 0 \end{bmatrix}^T = \begin{bmatrix} -a_{11} & -a_{21} & -a_{31} & 0 \\ -a_{12} / 57.3V_0 & -a_{22} / 57.3V_0 & -a_{32} / 57.3V_0 & 0 \end{bmatrix}^T;$$

the elements of the matrices are calculated with special equations (Lungu 2008), with respect to the stability derivates for the chosen aircraft type.

The calculus equations for the components of the wind velocity may be by the forms (Che and Chen 2001; FAA 1971):

$$V_{vx} = -V_{vx_0}\sin(\omega_0 t), V_{vz} = -V_{vz_0}\left[1-\cos(\omega_0 t)\right], \omega_0 = 2\pi / T_0 . \tag{23}$$

These relationships shape the wind shears; the aircraft, during the landing process, is disturbed by head wind and rear wind combined with vertical wind. In equation (23) T_0 is the flight time for the wind shear.

In most of the cases, some coefficients of the matrices $\mathbf{A}$ and $\mathbf{B}$ are negligible or null, for examples $a_{13}, b_{11}, a_{34},$ and b_{32}. As a result, the first and third state equations become:

$$\dot{V}_x = a_{11}V_x + a_{12}\alpha + a_{14}\theta + b_{12}\delta_T , \tag{24}$$

$$\dot{\omega}_y = a_{31}V_x + a_{32}\alpha + a_{33}\omega_y + b_{21}\delta_p . \tag{25}$$

The inverse dynamic model with respect to the state variables V_x and ω_y is described by the equations:

$$\delta_{p_c} = b_{31}^{-1}\left(\dot{\omega}_{y_c} - a_{31}V_x - a_{32}\alpha - a_{33}\omega_y\right), \tag{26}$$

$$\delta_{T_c} = b_{12}^{-1}\left(\dot{V}_{x_c} - a_{11}V_x - a_{12}\alpha - a_{14}\theta\right); \tag{27}$$

the variables "m_c" are the calculated values of variables "m".

The relationship between the aircraft pitch rate ω_y and the angular rates $\dot{\theta}$ and $\dot{\psi}$ (Lungu 2008) is the following one:

$$\omega_y = \dot{\theta}\cos\varphi + \dot{\psi}\cos\theta\sin\varphi ; \tag{28}$$

taking into account the above equation and that the aircraft lateral movement during the landing process is stabilized (the roll angle $\varphi = 0$), it follows $\dot{\omega}_{y_c} = \ddot{\theta}_c$ and the equation (25) becomes:

$$\delta_{p_c} = b_{21}^{-1}\left(\ddot{\theta}_c - a_{31}V_x - a_{32}\alpha - a_{33}\omega_y\right). \tag{29}$$

$\ddot{\theta}_c$ represents the calculated pitch angular acceleration (Kawaguchi et al. 2008), and θ_c is the calculated pitch angle, i.e. the command provided by the glide slope controller or by the flare controller.

IV. ALSs for Aircrafts Flight in Longitudinal Plane

In this section, two automatic landing systems (ALS) are proposed: 1) ALS with ILS system; and 2) ALS which controls the altitude by means of the state vector. The architectures of the two ALSs are shown in Figs 3 and 4. Fig.

3 presents the ALS with the control made by means of the variables $\Gamma, H,$ and V_x, while Fig. 4 shows the ALS which uses the state vector in the control algorithm, with the prescription of the GS starting point $A_p(x_p, H_p)$ coordinates. The two ALSs are based on the aircraft movement geometry described in Figs 1 and 2.a, and on the geometry of the aircraft movement in Fig. 2.b, respectively.

For the system in Fig. 3, the control law of the pitch angle (δ_{p_c}) has been chosen having a PD form, while, for the system in Fig. 4, a PID form was used. For the structure in Fig. 4, the command law δ_{p_c}, described by equation (28), is based on the dynamic inversion with $\ddot{\theta}_c$ by the form (Calise and Rysdyk 1999):

$$\dot{\omega}_{y_c} = \ddot{\theta}_c = \ddot{\bar{\theta}} + k_p^{\theta}(\bar{\theta} - \theta) + k_p^{\dot{\theta}}(\dot{\bar{\theta}} - \dot{\theta}) + k_{pi}^{\theta} \int (\bar{\theta} - \theta)\mathrm{d}t\,, \tag{30}$$

where $\bar{\theta}$ and its derivatives represent the state variables of the second order command filter, commanded by a PID controller. The second order state filter (the system with respect to the variable θ is a second order system) is described by the equation:

$$\ddot{\bar{\theta}} + 2\xi_0\omega_0\dot{\bar{\theta}} + \omega_0^2\bar{\theta} = \omega_0^2\theta_r\,, \tag{31}$$

with the reference angle θ_r given by the PID controller having the equation:

$$k_p^h(H_c - H) + k_{pi}^h \int (H_c - H)\mathrm{d}t + k_{pd}^h(\dot{H}_c - \dot{H}) = \theta_r\,. \tag{32}$$

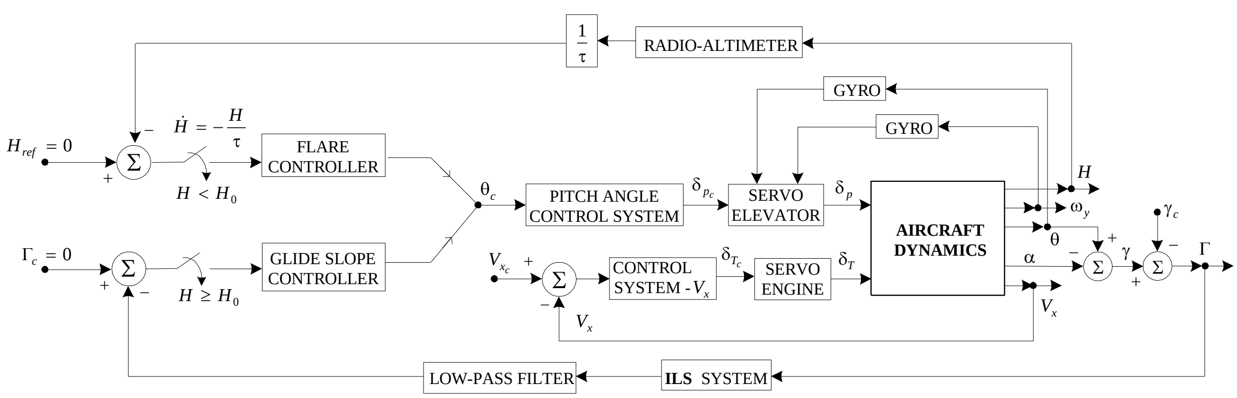

Fig. 3 ALS with the control made by means of variables Γ, H, and V_x

Similarly, the control law δ_{T_c}, of form (27), with $\dot{V}_{x_c}$ of the form:

$$\dot{V}_{x_c} = \dot{\bar{V}}_x + k_x(\bar{V}_x - V_x) + k_{xi} \int (\bar{V}_x - V_x)\mathrm{d}t \tag{33}$$

is based on the dynamic inversion principle (Pashilkar et al. 2006).

A particular form of the ALS based on the architecture in Fig. 3 is presented in Fig. 5. The glide slope controller is a PI controller, but, for a better stabilization, we add an element which introduces a phase advance (Lungu 2000). Therefore, the controller transfer function becomes:

$$H_c(\mathrm{s}) = k_c\left(1 + \frac{1}{T_c \mathrm{s}}\right)\frac{1 + T_1 \mathrm{s}}{1 + T_2 \mathrm{s}}. \tag{34}$$

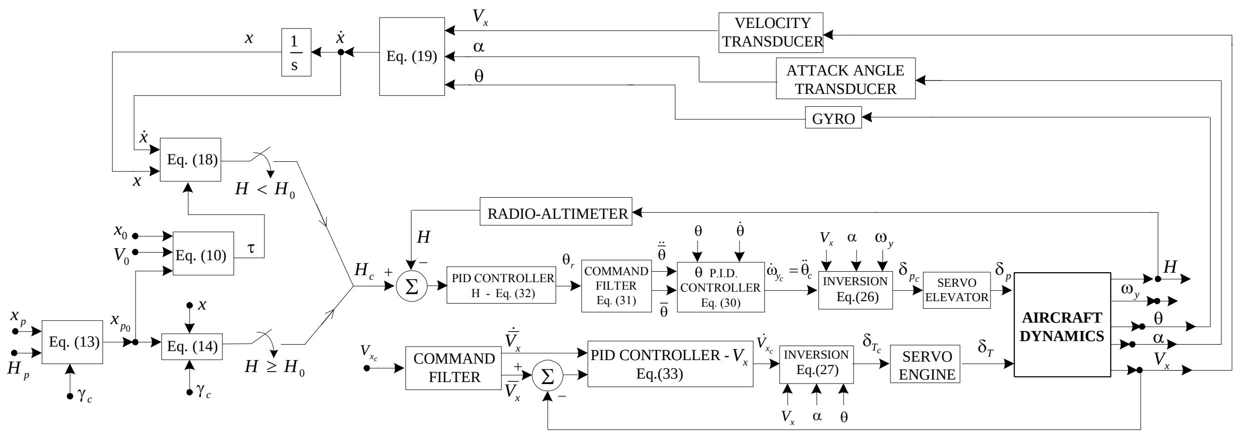

Fig. 4 ALS with the control made by means of the state vector

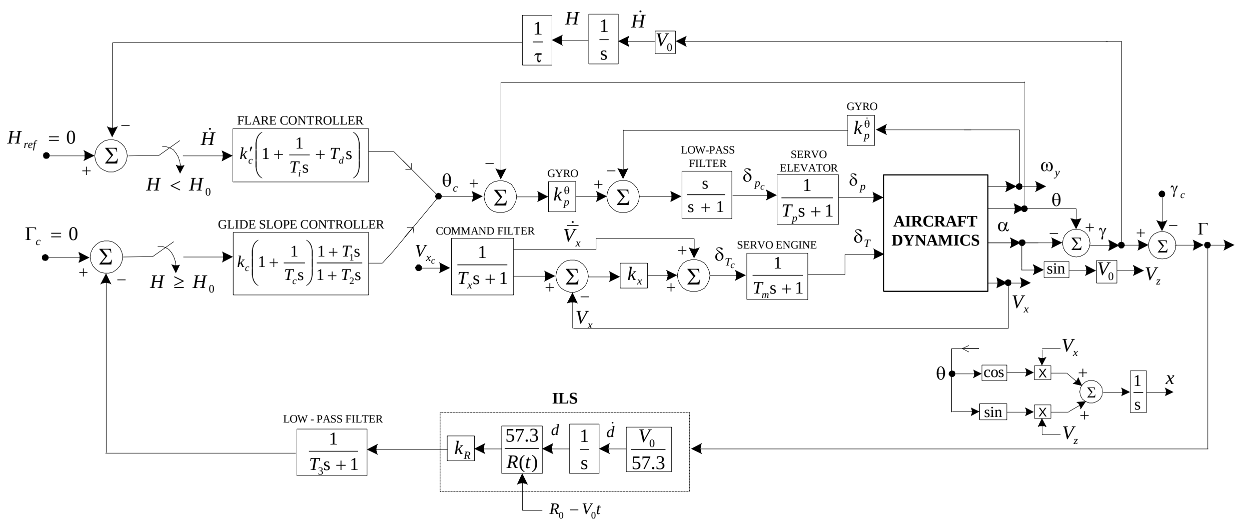

Fig. 5 ALS in longitudinal plane based on the block diagram in Fig. 3

The considered transfer function of the flare controller is:

$$H_c(\mathrm{s}) = k_c'\left(1 + \frac{1}{T_i \mathrm{s}} + T_d \mathrm{s}\right). \tag{35}$$

while the control law of the pitch angle has been chosen by a PD form. The gains of the angle gyro and of the angular rate gyro are k_p^{θ} and $k_p^{\dot{\theta}}$, respectively (Lungu 2000; Lungu 1997);

$$\delta_{p_c} = k_p^{\theta}(\theta_c - \theta) - k_p^{\dot{\theta}}\dot{\theta}. \tag{36}$$

On the other way, the control of the aircraft altitude on the flare trajectory is not made by using the altitude H; the control is made by means of the slope angle γ. Thus, according to aircraft cinematic equation (12), by controlling the slope angle γ we control $\dot{H}$ and H. To avoid the variation of the aircraft flight velocity, the component V_x of the aircraft velocity is controlled. The desired velocity V_{x_c} is the input of a first order command filter (the relative order is expressed with respect to V_x), while δ_{T_c} is a proportional control law:

$$\delta_{T_c} = \dot{\overline{V}}_x + k_x(\overline{V}_x - V_x); \tag{37}$$

$\overline{V}_x$ and $\dot{\overline{V}}_x$ are provided by the first order command filter.

The horizontal velocity $\dot{x}$ is obtained using the equation (19) and the aircraft horizontal displacement is obtained by the integration of $\dot{x}$. The transducer errors have little influence on the dynamic parameters of ALS (Lungu and Grigorie 2005; Grigorie 2007).

From the other point of view, in the conditions of strong aerodynamic disturbances, the control laws may become inefficient. That is why some adaptive components were added to the PID components of the control laws in Fig. 4. Usually, these adaptive control laws are based, for example, on the concept of dynamic inversion and neural networks (Singh and Padhi 2008; Che and Chen 2001; FAA 1971; Liao et al. 2005; Mori and Suzuki 2009; Niculescu 2001; MIT Open Course 2007; Kargin 2007; Vo and Sridhar 2008). Also, in order to improve the performances of the automatic control system, the controllers in Fig. 5 were replaced by fuzzy controllers and a comparative analysis was performed. All the considered cases for the two ALSs proposed architectures were tested through numerical simulation.

V. The Design of the Fuzzy Logic Controllers

Fuzzy logic is an innovative technology that provides a simple tool to interpret the human experience into reality. This enhances the conventional system design with engineering expertise. The fuzzy logic use can help to circumvent the need for rigorous mathematical modeling, which is a very difficult task, if not an impossible one. Fuzzy logic controllers are rule-based controllers. The basic configuration of a fuzzy logic model can be simply represented in four parts: the fuzzifier, the inference engine, the defuzzifier, and a knowledge base. The fuzzifier reads, measures, scales the control variable, and transforms the measured numerical values into the corresponding linguistic variables with appropriate membership values. The knowledge base includes the definitions of the fuzzy membership functions defined for each control variables and the necessary rules (IF-THEN rules) that specify the control goals using linguistic variables. The inference engine calls to the fuzzy rule base to derive the linguistic values for the output linguistic variables. The defuzzifier converts the inferred decision from the linguistic variables back to the numerical values. Therefore, the development of the control system based on fuzzy logic involves the following steps: fuzzification strategy; data base building; rule base elaboration; inference machine elaboration; deffuzification strategy (Tomescu 2001).

The simplest fuzzy controller is the proportional controller (FP), being relevant for state or output feedback in a state space controller. Its input is the error and the output is the control signal. From another perspective, derivative action helps to predict the error and the proportional-derivative (PD) controller uses the derivative action to improve closed-loop stability (Jantzen 1998). The equation of a PD controller can be expressed as follows:

$$i(t) = k_p \cdot e(t) + k_d \cdot \frac{\mathrm{d}e(t)}{\mathrm{d}t} = k_p \cdot \left[e(t) + T_d \cdot \frac{\mathrm{d}e(t)}{\mathrm{d}t} \right], \tag{38}$$

where $i(t)$ is the command variable in time, e is the operating error, k_p is the proportional gain and k_d is the derivative gain. The control signal is thus proportional to an estimate of the error T_d seconds ahead, where the estimate is obtained by linear extrapolation. If the T_d time constant is zero, the controller becomes a purely proportional one. The gradual increase of the T_d value will produce damped oscillations of the system, over a threshold value the system becoming over damped (Jantzen 1998).

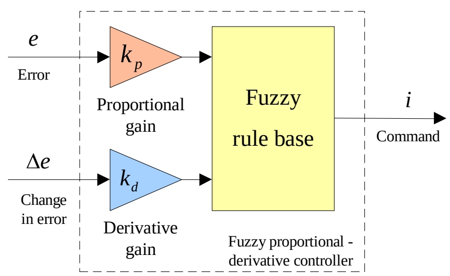

Fig. 6 FPD controller architecture

In a discrete form, the equation (38) becomes (Kumar et al. 2008):

$$i(k) = k_p \cdot e(k) + k_d \cdot \frac{[e(k) - e(k-1)]}{T_S}, \tag{39}$$

or

$$i(k) = k_p \cdot e(k) + k_d \cdot \Delta e(k). \tag{40}$$

k is the step, T_S – the sample period, and $\Delta e(k)$ – the change in error. So, the inputs of the fuzzy proportional-derivative (FPD) controller are the error and the derivative of the error (called the change in error) - Fig. 6.

Additionally, if there is a sustained error in steady state, an integral action is absolutely necessary. The integral component will increase the control signal if there is a positive error, or will decrease it if the error is negative in order to obtain zero error value in steady state (Jantzen 1998). Considering the control law of a proportional-integral (PI) controller is easily to find from its discrete form that for a fuzzy PI controller obtaining are also used the error and change in error as inputs to the rule base (Kumar 2008). Literature shows that it is rather difficult to write rules for the integral action because of the integrator windup problem emerging when the actuator has physical limitations; after saturation the control action stays constant, but the error will continue to be integrated and the integrator to wind up (Jantzen 1998). Here, there are proposed two methods to obtain a fuzzy controller with an integral component and avoid the integrator windup problem: a fuzzy incremental controller architecture (Fig. 7.a), respectively, a parallel integral action and fuzzy PD architecture (Fig. 7.b). Also, in (Kumar 2008) two equivalent architectures for a fuzzy PID controller are given: a) fuzzy PI + fuzzy PD in feedback mode; b) fuzzy PI + fuzzy PD cascade configuration. The disadvantage of the incremental controller in Fig.7.a is that it does not include the derivative component well (Jantzen 1998). So, to have all the benefits of a PID control in a simple manner it is recommended to choose the structure in Fig. 7.b for FLC.

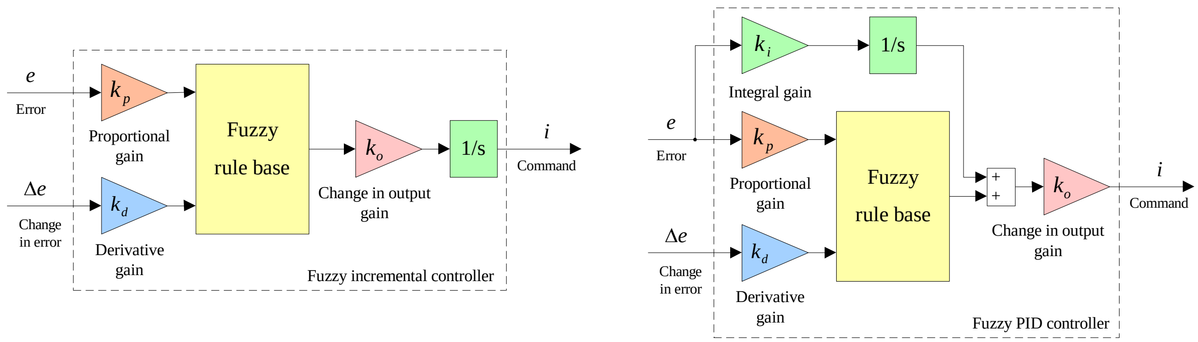

a. b.

Fig. 7 Architectures for fuzzy controllers with integral component

For the first FLC (first phase of the landing process) there was chosen the fuzzy proportional-integral-derivative (FPID) structure in Fig.7.b. Also, the [-1, 1] interval was chosen like universe for all of the input and output signals. After some numerical simulations we had opted for a number of three membership functions for each of the two inputs, and five membership functions for the output. The shapes chosen for inputs membership functions were *s*-function, π-function, respectively *z*-function. Generally, an *s*-function shaped membership function can be implemented using a cosine function:

$$s(\bar{x}_{left}, \bar{x}_{right}, \bar{x}) = \begin{cases} 0, & \text{if} \quad \bar{x} < \bar{x}_{left} \\ \dfrac{1}{2}\left[1 + \cos\left(\dfrac{\bar{x} - \bar{x}_{right}}{\bar{x}_{right} - \bar{x}_{left}}\pi\right)\right], & \text{if} \quad \bar{x}_{left} \le \bar{x} \le \bar{x}_{right}, \\ 1, & \text{if} \quad \bar{x} > \bar{x}_{right} \end{cases} \tag{41}$$

a *z*-function shaped membership function is a reflection of an *s*-function shaped one:

$$z(\bar{x}_{left}, \bar{x}_{right}, \bar{x}) = \begin{cases} 1, & \text{if} \quad \bar{x} < \bar{x}_{left} \\ \dfrac{1}{2}\left[1 + \cos\left(\dfrac{\bar{x} - \bar{x}_{left}}{\bar{x}_{right} - \bar{x}_{left}}\pi\right)\right], & \text{if} \quad \bar{x}_{left} \le \bar{x} \le \bar{x}_{right}, \\ 0, & \text{if} \quad \bar{x} > \bar{x}_{right} \end{cases} \tag{42}$$

and a π -function shaped membership function is a combination between the first two:

$$\pi(\bar{x}_{left}, \bar{x}_{m1}, \bar{x}_{m2}, \bar{x}_{right}, \bar{x}) = \min[s(\bar{x}_{left1}, \bar{x}_{m1}, \bar{x}),\; z(\bar{x}_{m2}, \bar{x}_{right}, \bar{x})], \tag{43}$$

with the peak flat over the $[\bar{x}_{m1}, \bar{x}_{m2}]$ middle interval. $\bar{x}$ is the independent variable on the universe, $\bar{x}_{left}$ is the left breakpoint, and $\bar{x}_{right}$ is the right breakpoint (Jantzen 1998).

To define the rules, there was chosen a Sugeno fuzzy model, a model proposed by Takagi, Sugeno and Kang (Mahfouf et al. 1999). A Takagi, Sugeno and Kang fuzzy rule, for a two input - single output system, is of the following form:

$$\text{"if } (\bar{x}_1 \text{ is A) and } (\bar{x}_2 \text{ is B) then } y = f(\bar{x}_1, \bar{x}_2)\text{"}, \tag{44}$$

where A and B are fuzzy sets in the antecedent, and $y = f(\bar{x}_1, \bar{x}_2)$ is a crisp function in the consequent; $f(\bar{x}_1, \bar{x}_2)$ is a polynomial function. If *f* is a first order polynomial, then the resulting fuzzy inference is called a first order Sugeno fuzzy model, while if *f* is a constant then it is a zero-order Sugeno fuzzy model. For a two input - single output system, there is given a first-order Sugeno fuzzy model, with *N* rules by (Mahfouf et al. 1999):

$$\begin{array}{l}
\text{Rule } 1: \;\text{If } \bar{x}_1 \text{ is } \mathrm{A}_1^1 \text{ and } \bar{x}_2 \text{ is } \mathrm{A}_2^1, \text{ then } y^1(\bar{x}_1, \bar{x}_2) = b_0^1 + a_1^1\bar{x}_1 + a_2^1\bar{x}_2, \\
\vdots \\
\text{Rule } i: \;\text{If } \bar{x}_1 \text{ is } \mathrm{A}_1^i \text{ and } \bar{x}_2 \text{ is } \mathrm{A}_2^i, \text{ then } y^i(\bar{x}_1, \bar{x}_2) = b_0^i + a_1^i\bar{x}_1 + a_2^i\bar{x}_2, \\
\vdots \\
\text{Rule } N: \;\text{If } \bar{x}_1 \text{ is } \mathrm{A}_1^N \text{ and } \bar{x}_2 \text{ is } \mathrm{A}_2^N, \text{ then } y^N(\bar{x}_1, \bar{x}_2) = b_0^N + a_1^N\bar{x}_1 + a_2^N\bar{x}_2,
\end{array} \tag{45}$$

where $\bar{x}_q\ (q = \overline{1,2})$ are the individual input variables, $y^i\ (i = \overline{1,N})$ is the first-order polynomial function in the consequent, and $\mathrm{A}_q^i\ (i = \overline{1,N})$ are the associated individual antecedent fuzzy sets of each input variable.

$a_k^i\ (k = \overline{1,2},\ i = \overline{1,N})$ are the parameters of the linear function and $b_0^i\ \ (i = \overline{1,N})$ denotes a scalar offset.

For any input vector, $\bar{\boldsymbol{x}} = [\bar{x}_1,\ \bar{x}_2]^T$, if the singleton fuzzifier, the product fuzzy inference and the center average defuzzifier are applied (Sugeno), then the output of the fuzzy model y is inferred as follows (weighted average):

$$y = \left(\sum_{i=1}^{N} w^i(\bar{\boldsymbol{x}})y^i\right) \Big/ \left(\sum_{i=1}^{N} w^i(\bar{\boldsymbol{x}})\right). \tag{46}$$

$$w^i(\boldsymbol{x}) = \mathrm{A}_1^i(\bar{x}_1) \times \mathrm{A}_2^i(\bar{x}_2) \tag{47}$$

represents the degree of fulfillment of the antecedent, i.e., the level of firing of i^{th} rule.

In the [-1, 1] universe interval, a three range partition, negative (N), zero (Z) and positive (P), were chosen for the inputs e and Δe, and five-range partition, negative-big (NB), negative-small (NS), zero (Z), positive-small (PS) and positive-big (PB) were used for the output. According to the values in Table 1, the membership functions for both inputs are under the form depicted in Fig. 8, and are given by equations (41), (42) or (43):

$$A_1^1(\bar{x}) = A_2^1(\bar{x}) = z(-1,0,\bar{x}) = \begin{cases} 1, & \text{if } \bar{x} < -1 \\ \frac{1}{2}\left[1+\cos(\bar{x}+1)\pi\right], & \text{if } -1 \le \bar{x} \le 0, \\ 0, & \text{if } \bar{x} > 0 \end{cases} \quad (48)$$

$$A_1^2(\bar{x}) = A_2^2(\bar{x}) = \min[s(-1,0,\bar{x}),\ z(0,1,\bar{x})] = \begin{cases} 0, & \text{if } \bar{x} < -1 \\ \frac{1}{2}\left[1+\cos(\pi\bar{x})\right], & \text{if } -1 \le \bar{x} \le 1, \\ 0, & \text{if } \bar{x} > 1 \end{cases} \quad (49)$$

$$A_1^3(\bar{x}) = A_2^3(\bar{x}) = s(0,1,\bar{x}) = \begin{cases} 0, & \text{if } \bar{x} < 0 \\ \frac{1}{2}\left[1+\cos(\bar{x}-1)\pi\right], & \text{if } 0 \le \bar{x} \le 1, \\ 1, & \text{if } \bar{x} > 1 \end{cases} \quad (50)$$

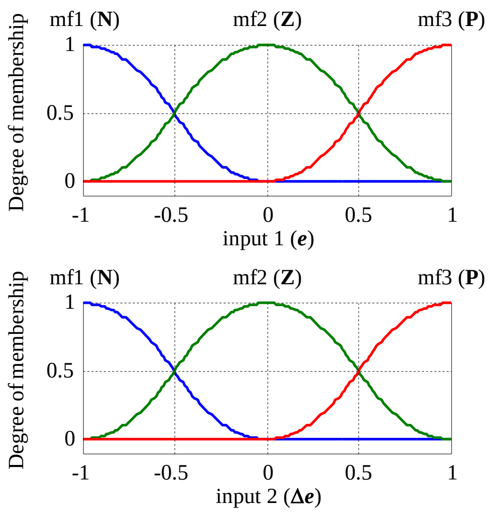

Fig. 8 Membership functions and rule-based inference for the first landing phase FLC

Table 1 Parameters of the inputs membership functions for the first landing phase FLC

	mf type	*mf* parameters			
		$\bar{x}_{left}$	$\bar{x}_{m1}$	$\bar{x}_{m2}$	$\bar{x}_{right}$
*mf*1 (A_1^1 and A_2^1)	*z*-function	-1	-	-	0
*mf*2 (A_1^2 and A_2^2)	π -function	-1	0	0	1
*mf*3 (A_1^3 and A_2^3)	*s*-function	0	-	-	1

For the output membership functions, constant values were chosen (NB=-1, NS=-0.5, Z=0, PS=0.5, PB=1), so the values of a_k^i ($k = \overline{1,2}$, $i = \overline{1,N}$) parameters in equation (45) are zero. Starting from the membership functions of the input and output, a set of 9 inference rules were derived (N=9):

$$
\begin{aligned}
&\text{Rule 1: If } e \text{ is } A_1^1 \text{ and } \Delta e \text{ is } A_2^1, \text{ then } y^1(e,\Delta e) = -1,\\
&\text{Rule 2: If } e \text{ is } A_1^1 \text{ and } \Delta e \text{ is } A_2^2, \text{ then } y^2(e,\Delta e) = -0.5,\\
&\text{Rule 3: If } e \text{ is } A_1^1 \text{ and } \Delta e \text{ is } A_2^3, \text{ then } y^3(e,\Delta e) = 0,\\
&\text{Rule 4: If } e \text{ is } A_1^2 \text{ and } \Delta e \text{ is } A_2^1, \text{ then } y^4(e,\Delta e) = -0.5,\\
&\text{Rule 5: If } e \text{ is } A_1^2 \text{ and } \Delta e \text{ is } A_2^2, \text{ then } y^5(e,\Delta e) = 0,\\
&\text{Rule 6: If } e \text{ is } A_1^2 \text{ and } \Delta e \text{ is } A_2^3, \text{ then } y^6(e,\Delta e) = 0.5,\\
&\text{Rule 7: If } e \text{ is } A_1^3 \text{ and } \Delta e \text{ is } A_2^1, \text{ then } y^7(e,\Delta e) = 0,\\
&\text{Rule 8: If } e \text{ is } A_1^3 \text{ and } \Delta e \text{ is } A_2^2, \text{ then } y^8(e,\Delta e) = 0.5,\\
&\text{Rule 9: If } e \text{ is } A_1^3 \text{ and } \Delta e \text{ is } A_2^3, \text{ then } y^9(e,\Delta e) = 1.
\end{aligned}
\tag{51}
$$

The rule-based inference chosen for each consequent is also represented in Fig. 9. From the previous considerations, the fuzzy control surface results under the form represented in Fig. 10.

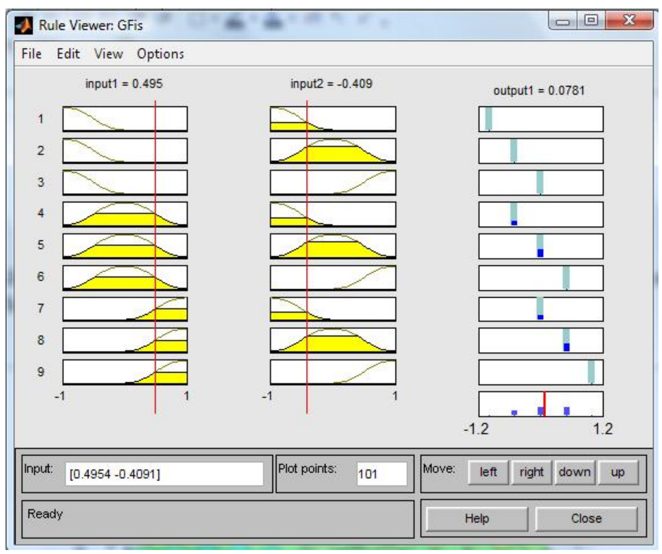

Fig. 9 The rule-based inference for the first landing phase FLC

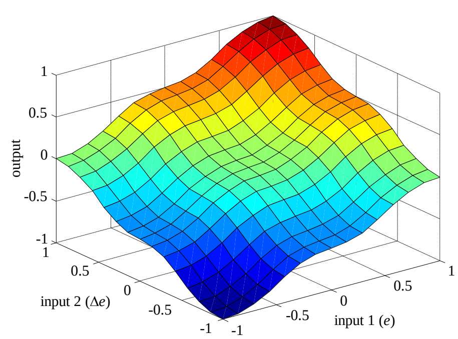

Fig. 10 The fuzzy control surface for the first landing phase FLC

For the second FLC (the second phase of the landing process) there was chosen the fuzzy proportional-derivative (FPD) structure in Fig. 6. The [-1, 1] interval resulted like universe for all of the input signals, while [-4, 0.2] interval was chosen like universe for the output signal. As in the first FLC case, we had opted for a number of three membership functions for each of the two inputs, and four membership functions for the output. The shapes chosen for the input membership functions were, also, *s*-function, *π*-function, respectively *z*-function; the membership functions for both inputs are by the form depicted in Fig. 8, and are given by the equations (41), (42) or (43). The parameters of these membership functions are similar with those chosen for the first lading phase FLC (see Table 1).

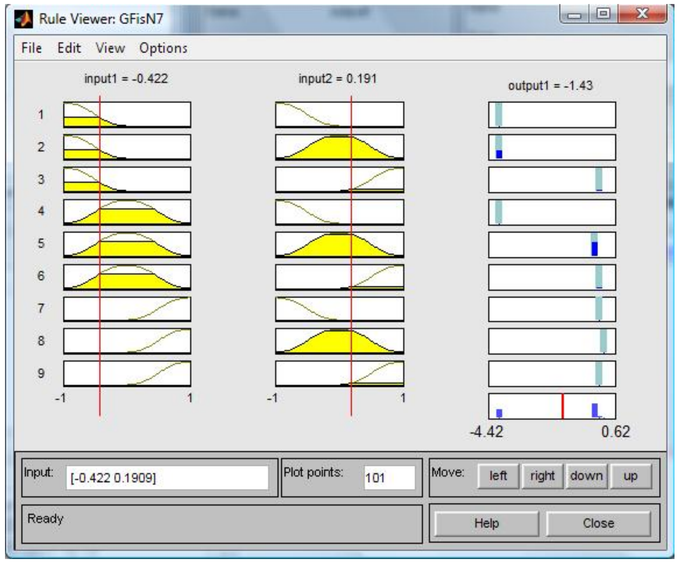

Fig. 11 The rule-based inference for the second landing phase FLC

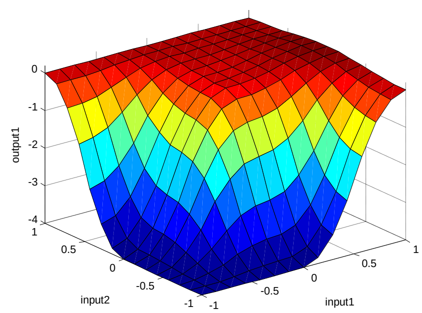

Fig. 12 The fuzzy control surface for the second landing phase FLC

For the output membership functions, constant values were chosen (NB=-4, NS=-0.18, Z=0, P=0.2), and a set of 9 inference rules were derived (N=9):

$$
\begin{aligned}
&\text{Rule 1: If } e \text{ is } \mathrm{A}_1^1 \text{ and } \Delta e \text{ is } \mathrm{A}_2^1, \text{ then } y^1(e,\Delta e) = -4,\\
&\text{Rule 2: If } e \text{ is } \mathrm{A}_1^1 \text{ and } \Delta e \text{ is } \mathrm{A}_2^2, \text{ then } y^2(e,\Delta e) = -4,\\
&\text{Rule 3: If } e \text{ is } \mathrm{A}_1^1 \text{ and } \Delta e \text{ is } \mathrm{A}_2^3, \text{ then } y^3(e,\Delta e) = 0,\\
&\text{Rule 4: If } e \text{ is } \mathrm{A}_1^2 \text{ and } \Delta e \text{ is } \mathrm{A}_2^1, \text{ then } y^4(e,\Delta e) = -4,\\
&\text{Rule 5: If } e \text{ is } \mathrm{A}_1^2 \text{ and } \Delta e \text{ is } \mathrm{A}_2^2, \text{ then } y^5(e,\Delta e) = -0.18,\\
&\text{Rule 6: If } e \text{ is } \mathrm{A}_1^2 \text{ and } \Delta e \text{ is } \mathrm{A}_2^3, \text{ then } y^6(e,\Delta e) = 0,\\
&\text{Rule 7: If } e \text{ is } \mathrm{A}_1^3 \text{ and } \Delta e \text{ is } \mathrm{A}_2^1, \text{ then } y^7(e,\Delta e) = 0,\\
&\text{Rule 8: If } e \text{ is } \mathrm{A}_1^3 \text{ and } \Delta e \text{ is } \mathrm{A}_2^2, \text{ then } y^8(e,\Delta e) = 0.2,\\
&\text{Rule 9: If } e \text{ is } \mathrm{A}_1^3 \text{ and } \Delta e \text{ is } \mathrm{A}_2^3, \text{ then } y^9(e,\Delta e) = 0.
\end{aligned}
\tag{52}
$$

The rule-based inference, chosen for each consequent, is presented in Fig. 11, while the resulted fuzzy control surface has the form in Fig. 12.

VI. Numerical Simulation Results

For the study of the ALS dynamics, we consider a Charlie-1 aircraft with the following stability derivates (Donald 1990):

$$
\begin{aligned}
&X_u = -0.021\,[1/\mathrm{s}],\ X_w = 0.122\,[1/\mathrm{s}],\ Z_u = -0.2\,[1/\mathrm{s}],\ Z_w = -0.512\,[1/\mathrm{s}],\ V_0 \cong V_{x_0} = 67\,[\mathrm{m/s}],\\
&N_w = -0.006\,[\mathrm{deg}/(\mathrm{s}\cdot\mathrm{m})],\ N_{\dot{w}} = -8\cdot 10^{-4}\,[\mathrm{deg/m}],\ X_{\delta_T} = 3.66\cdot 10^{-6}\,[(\mathrm{m/s})/\mathrm{deg}],\\
&Z_{\delta_T} = -1.69\cdot 10^{-7}\,[(\mathrm{m/s})/\mathrm{deg}],\ N_{\delta_T} \cong 0,\ Z_{\delta_p} = -1.96\,[(\mathrm{m/s})/\mathrm{deg}],\ N_{\delta_p} = 0,\ \sin\theta_0 \cong 0,\ \cos\theta_0 \cong 1,\ Z_u^* = Z_u / V_0 .
\end{aligned}
\tag{53}
$$

With these, the matrices (22) become:

$$
\mathbf{A} = \begin{bmatrix} -0.021 & 0.122 & 0 & -9.69 \\ -0.003 & -0.7535 & 1 & 0 \\ 0.000052 & -0.24569 & -0.213 & 0 \\ 0 & 0 & 1 & 0 \end{bmatrix},\ \mathbf{B} = \begin{bmatrix} 0 & 0.1 \\ -0.166 & 0 \\ -1.8 & 0 \\ 0 & 0 \end{bmatrix}. \tag{54}
$$

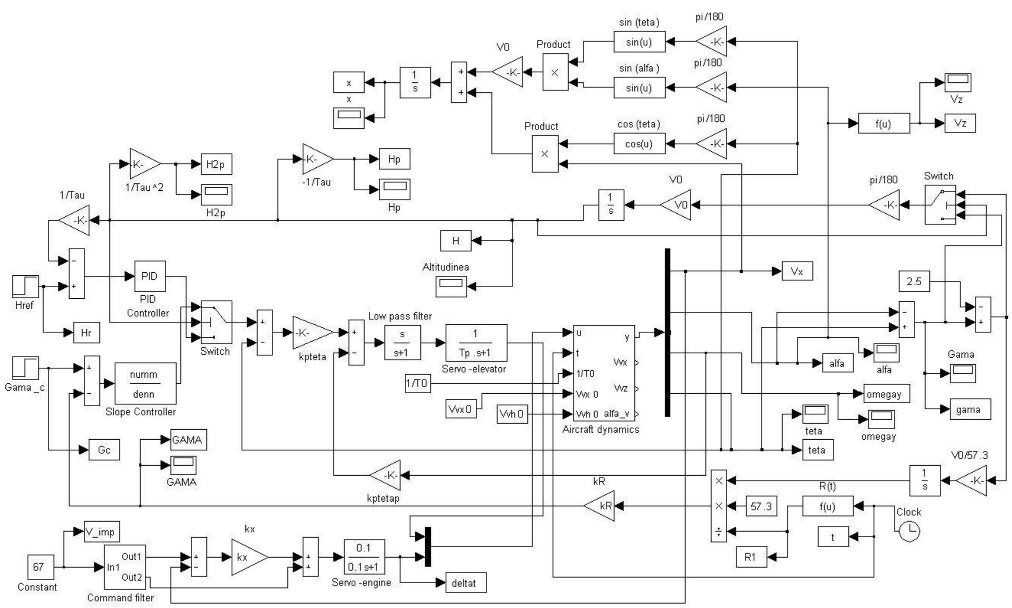

Fig. 13 Matlab/Simulink model for ALS with ILS system

The altitude at which the glide slope landing phase begins is $H_p = 320\,\mathrm{ft} \cong 100\,\mathrm{m}$. For the system in Fig. 5, we choose:

$$
\begin{aligned}
&k_p^{\theta} = -16,\ k_p^{\dot{\theta}} = -4\,[\mathrm{deg}/(\mathrm{deg/s})],\ k_c = -20\,[\mathrm{deg/V}],\ k_R = 0.01\,[\mathrm{V/deg}],\ k_x = 4\cdot 10^4,\\
&V_{x_c} = 67\,[\mathrm{m/s}],\ T_c = 30\,[\mathrm{s}],\ T_1 = 0.4\,[\mathrm{s}],\ T_2 = 0.04\,[\mathrm{s}],\ T_p = 0.1\,[\mathrm{s}],\ T_m = 0.1\,[\mathrm{s}],\\
&T_x = 6\,[\mathrm{s}],\ T_3 = 1\,[\mathrm{s}],\ k_c' = -1.5\,[\mathrm{deg}/(\mathrm{m/s})],\ T_i = 7.5\cdot 10^3\,[\mathrm{s}],\ T_d = 0.9\,[\mathrm{s}].
\end{aligned}
\tag{55}
$$

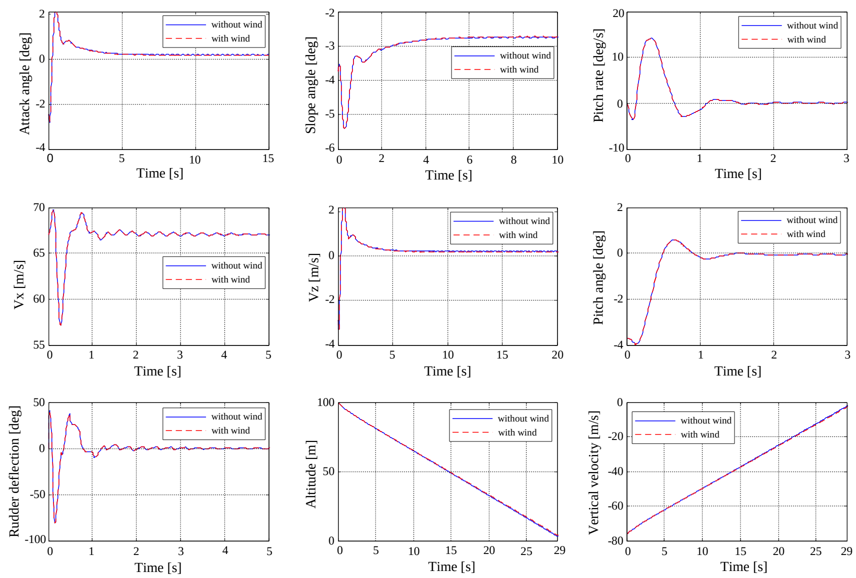

Fig. 14 The main variables of the ALS with ILS system in glide slope phase, with conventional controllers

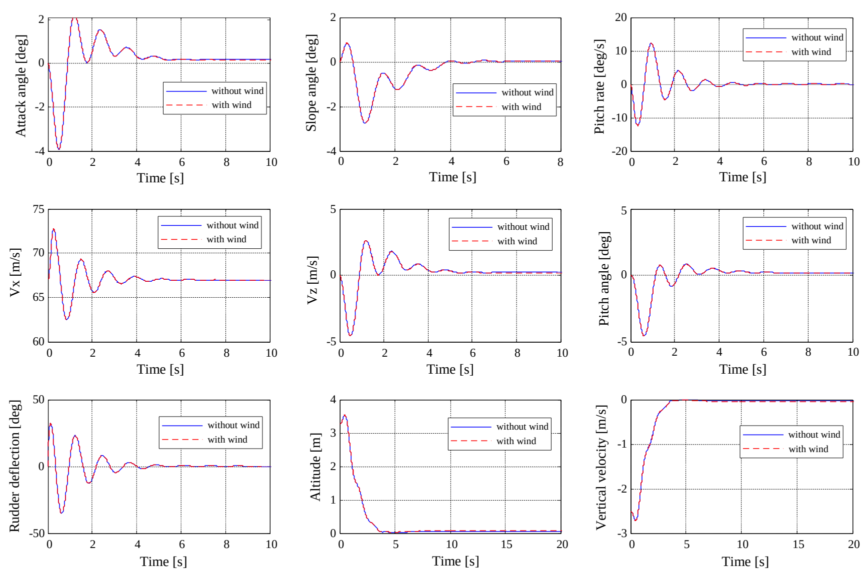

Fig. 15 The main variables of the ALS with ILS system in flare phase, with conventional controllers

Fig. 13 presents the Matlab/Simulink model for the system in Fig. 5. Firstly, the conventional controllers were used. In Fig. 14 and Fig. 15 are shown the dynamics of the main variables of the automatic control system, for the glide slope phase and for the flare phase, respectively, while in Fig. 16 the dependence $H = H(x)$ is depicted. The characteristics have been represented in the presence or in the absence of the wind shears ($V_{vx_0} = 10 m/s$, $V_{vz_0} = 15\, m/s, T_0 = 60\, s$). The presence of the wind shears is not very visible – the curves with solid line (without wind) overlap almost perfectly over the curves plotted with dashed line (with wind). The glide slope landing phase takes approximately 30 seconds; the time origin for the flare trajectory is chosen zero when the altitude is $H = H_0 = 3.25\,m$ (the altitude at which the glide slope process ends).

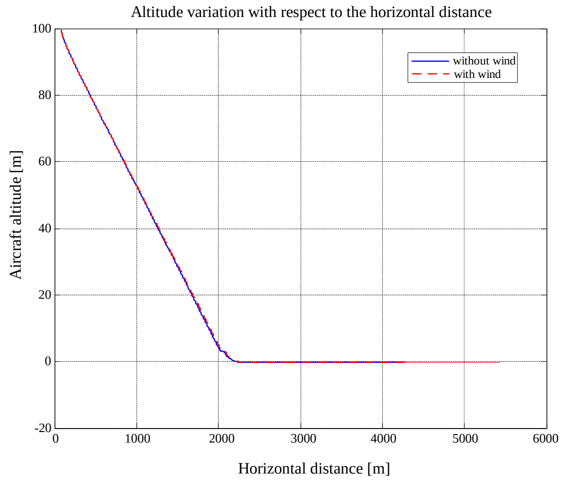

Fig. 16 The landing trajectory $H = H(x)$ for ALS with ILS system which uses conventional controllers

From the numerical simulations can be observed that, at the beginning of the landing phases, the variables have big amplitudes. That thing is due to the fact that the considered initial conditions were easily different by the trim conditions for the stability derivatives used in simulations and given in equation (53).

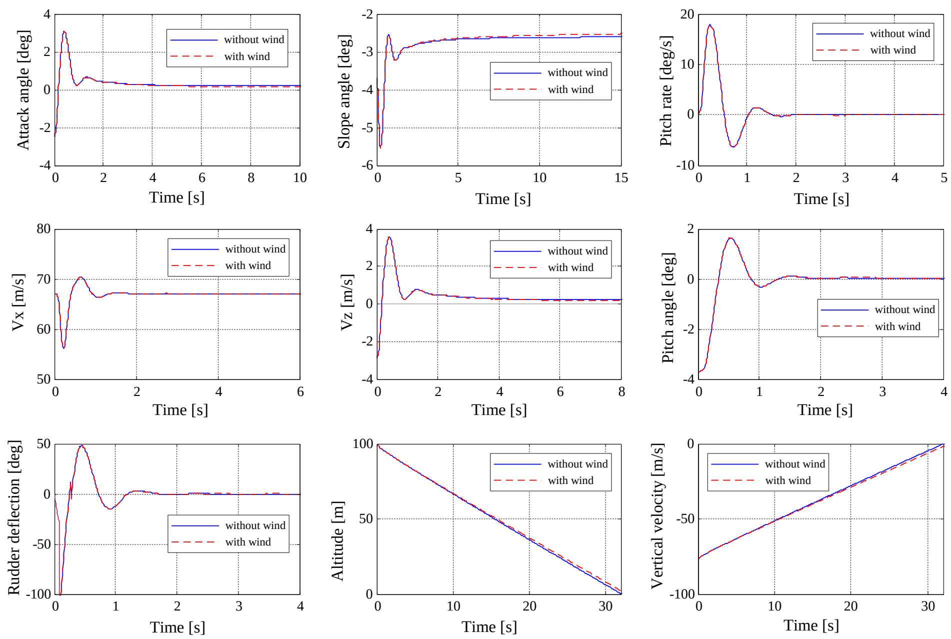

Fig. 17 The main variables of the ALS with ILS system in glide slope phase, with fuzzy controllers

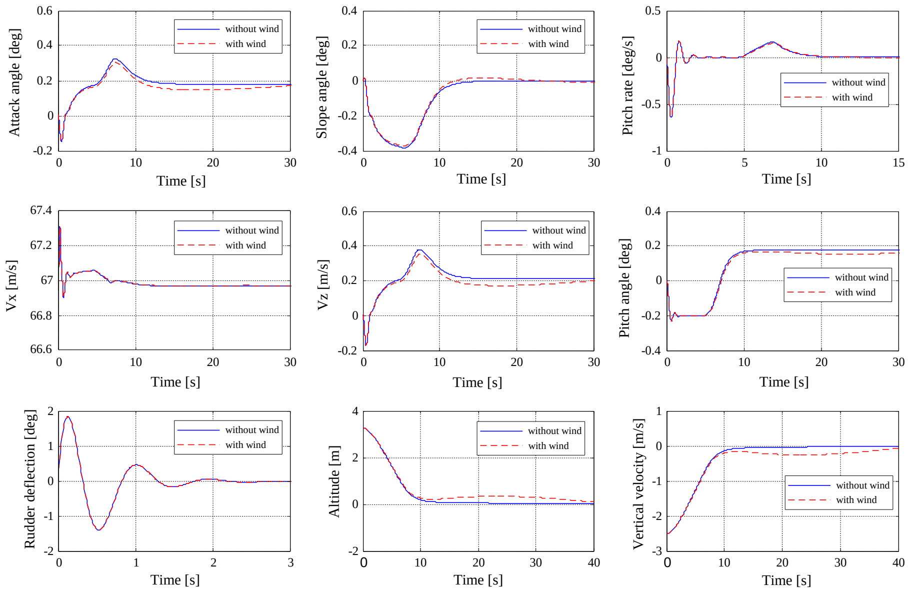

Fig. 18 The main variables of the ALS with ILS system in flare phase, with fuzzy controllers

If the conventional controllers for the ALS architecture in Fig. 5 are replaced by the previously designed fuzzy controllers, superior characteristics in terms of their dynamic and stationary qualities are obtained; this issue can be seen from the comparative analysis of the graphical characteristics in Fig. 14, and Fig. 15, with the equivalent characteristics in Fig. 17, and Fig. 18, respectively.

The wind shears insignificantly affect the transient regime of the two landing phases – the differences between the solid curves and the dashed ones are minor; the steady regime is not affected (the steady values of the variables are the same). The trajectories $H(t)$ are less influenced by the wind shears. The transient regime period is approximately the same for the two cases (with or without taking into consideration the wind shears).

In the above simulations we did not take into consideration the errors of the sensors (used for the measurement of the state variables). These errors are considered within simulation below.

For the gyro sensors, we consider the model of the error that takes into account the parameters from the data sheets offered by the sensors producers; the model of the error is described by the equation:

$$\omega = (\omega_i + S \cdot a_r + \overline{B} + \nu)\left(1 + \frac{\Delta K}{K}\right), \tag{56}$$

where ω is the output angular rate (the perturbed signal), $\omega_i -$ the input angular rate, $S -$ the sensibility to the acceleration a_r applied along an arbitrary direction, $\overline{B} -$ the bias, $K -$ the scale factor, $\Delta K -$ the calibration error of the scale factor, and $\nu -$ the noise of the sensor.

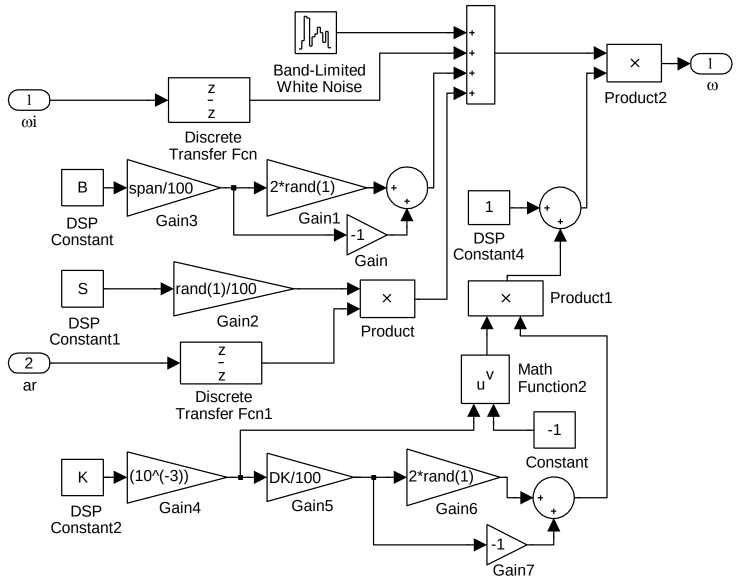

Fig. 19 The error model for the gyro in Matlab/Simulink

Implementing the equation (56) in Matlab/Simulink, the model in Fig. 19 has been obtained. It considers that in sensors data sheets the bias is given by its maximum value $\overline{B}$ as percentage of the span, the calibration error of the scale factor is given by its absolute maximum value ΔK as percentage of K, while the noise is given by using its maximum density value. Using the Matlab function "rand(1)" one generates the bias by a random value in the interval $(-\overline{B},\ \overline{B})$, the sensibility S in the interval $(0, S)$, and the calibration error of the scale factor in the interval $(-\Delta K,\ \Delta K)$. The noise is generated by using the Simulink block "Band-Limited White Noise" and the Matlab function "RandSeed" which generates a random value of its density in the interval $(80\% \cdot \nu_d,\ \nu_d)$.

The inputs of the error model are the angular rate ω_i, applied along the sensor sensibility axis, and the acceleration a_r, considered to be the resultant acceleration signal that acts upon the carry vehicle, while the output is the disturbed angular rate ω. In the numerical simulation, the following sensor parameters have been used: the noise density $0.1\left[(\deg/\ s)/\sqrt{Hz}\right]$, the bias $5\left[\deg/\ s\right]$, the error of the scale factor $1\% \cdot K$, the sensibility to accelerations $0.18\left[(\deg/\ s)/\ g\right]$; $\vec{g}$ is the gravitational acceleration.

For the structure in Fig. 5, with fuzzy controllers, taking into account or not the errors of the sensor, the characteristics in Figs 20 to 22 are obtained (a – sensor without errors, b – sensor with errors). The first 30 seconds of the landing process correspond to the glide slope phase, while the next 12 seconds correspond to the flare phase. Fig. 23 presents the curves $H = H(x)$ for the variant with fuzzy controllers, with or without wind shears, with or without considering the errors of the gyro sensor.

The sensor errors produce an increase of the signals amplitude in the transient regime and very small oscillations in the steady regime, but these errors do not affect the two landing phases.

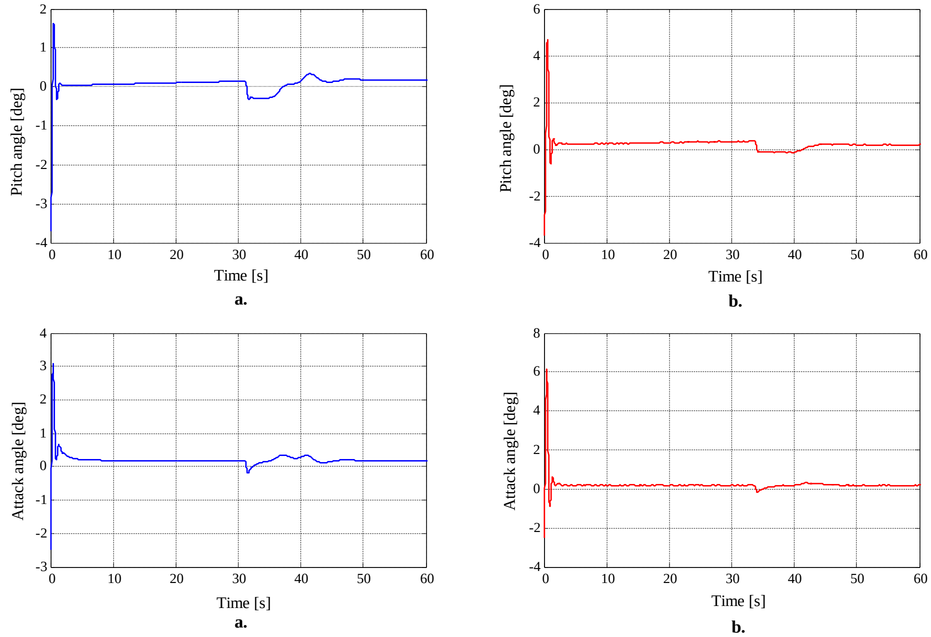

Fig. 20 The families of characteristics $\theta(t)$ and $\alpha(t)$ for the system in Fig. 5 (a – sensor without errors, b – sensor with errors)

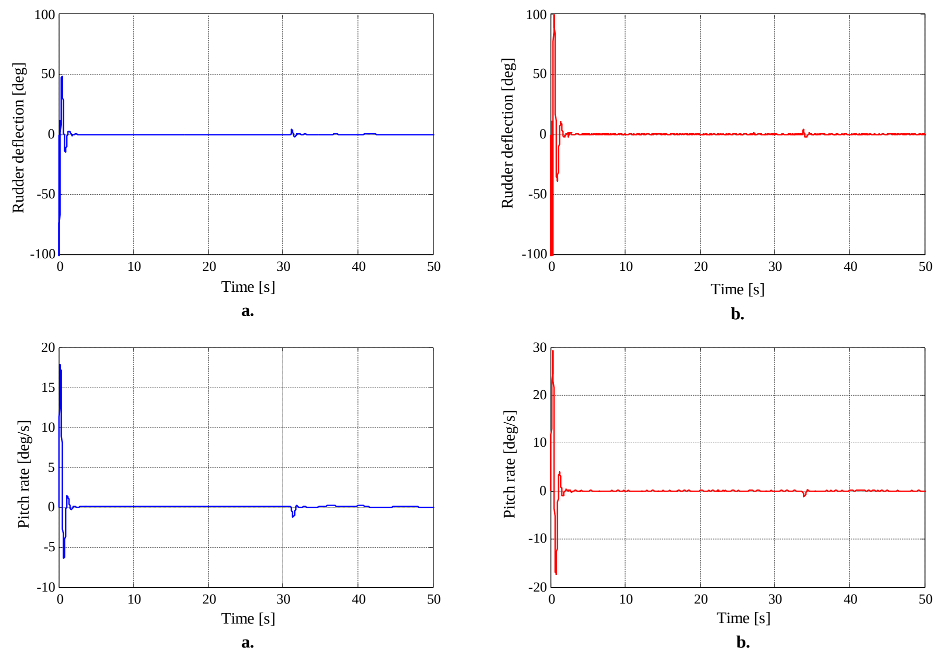

Fig. 21 The families of characteristics $\delta_p(t)$ and $\omega_y(t)$ for the system in Fig. 5 (a – sensor without errors, b – sensor with errors)

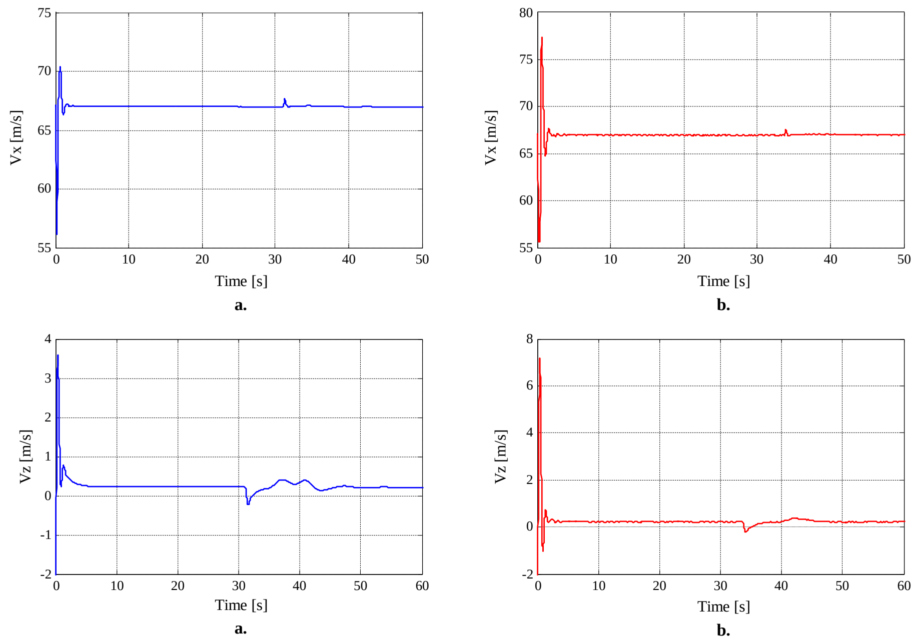

Fig. 22 The families of characteristics $V_x(t)$ and $V_z(t)$ for the system in Fig. 5 (a – sensor without errors, b – sensor with errors)

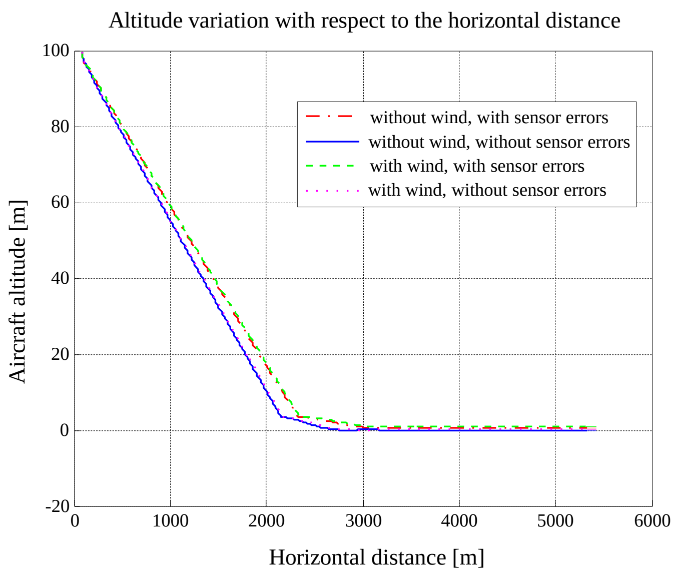

Fig. 23 The landing trajectory $H = H(x)$ by using fuzzy controllers with or without wind shears, with or without considering the errors of the gyro sensor

The second proposed ALS (based on the dynamic inversion concept) Matlab/Simulink model can be seen in Fig. 24 (based on the architecture in Fig. 4). Also, in Figs 25 and 26 are shown the dynamics of the main variables of the automatic control system, for the glide slope phase and for the flare phase, respectively, while in Fig. 27 is depicted the dependence $H = H(x)$. The used controller is a PID one, with the parameters:

$$k_p^h = 0.5\left[\deg/\,m\right], k_i^h = 10^{-4}\left[\deg/(m\cdot s)\right], k_d^h = 0.5\left[\deg/(\deg/\,s)\right]. \tag{57}$$

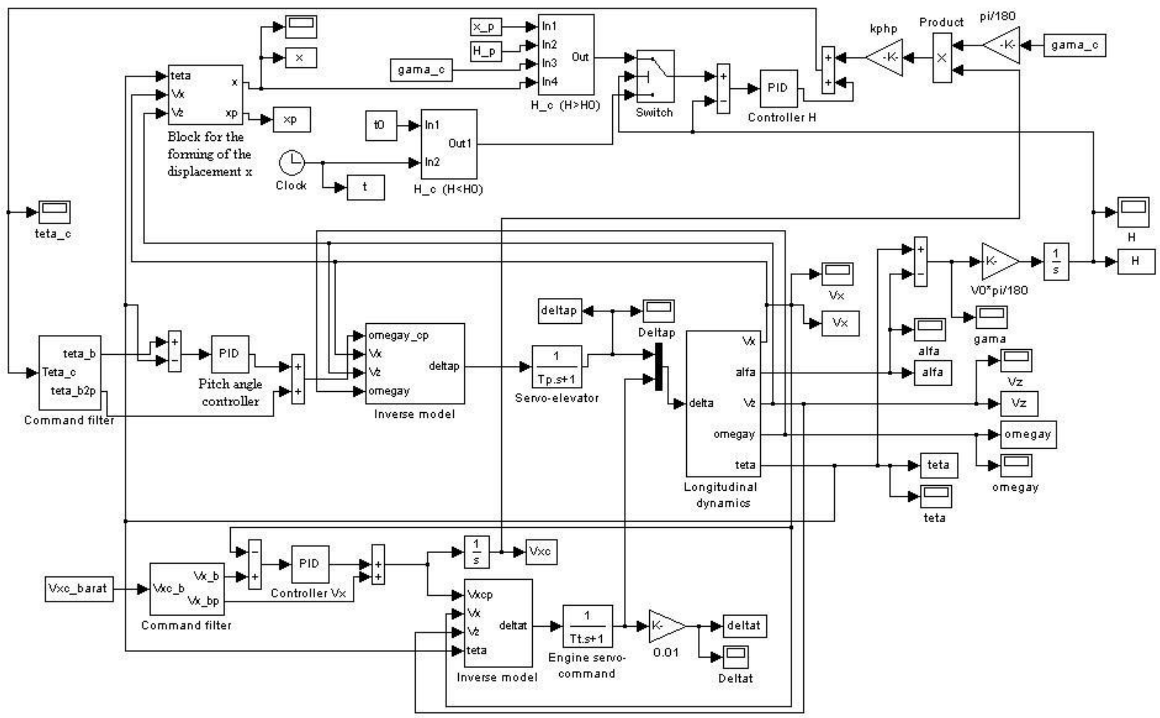

Fig. 24 The Matlab/Simulink model for the system in Fig. 4 – ALS based on the dynamic inversion concept

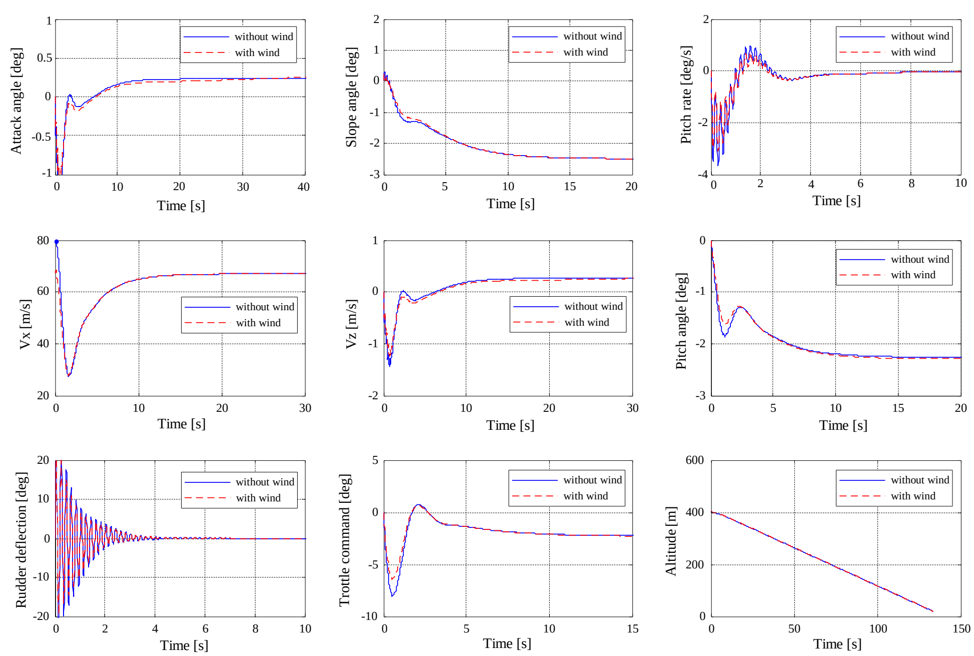

Fig. 25 The time characteristics in the glide slope phase for the ALS based on the dynamic inversion concept

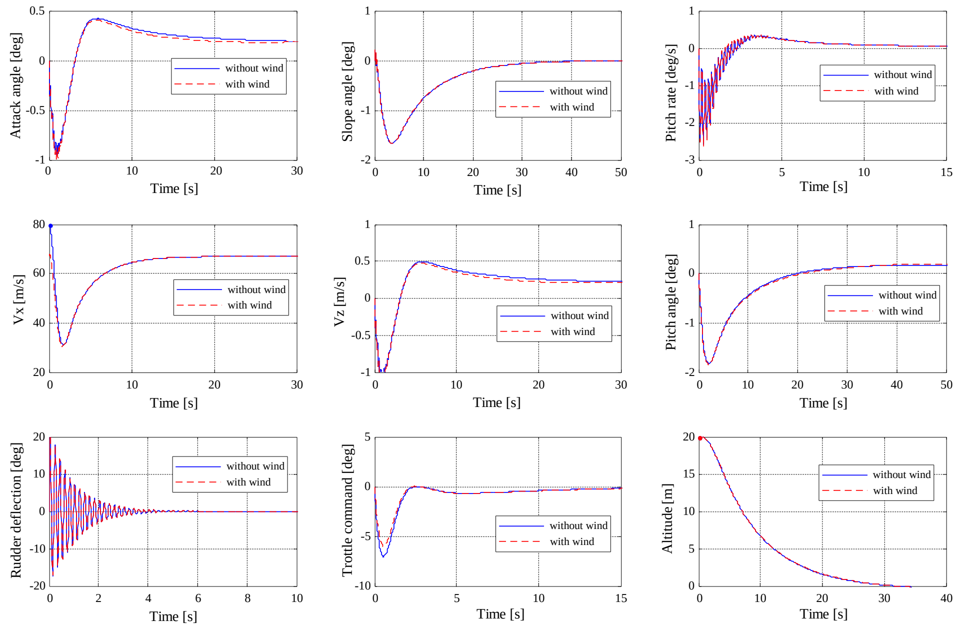

Fig. 26 The time characteristics in the flare phase for the ALS based on the dynamic inversion concept

Similar with the previously simulated cases (ALS with ILS system), the considered initial conditions were easily different by the trim conditions for the stability derivatives used in simulations and given in equation (53).

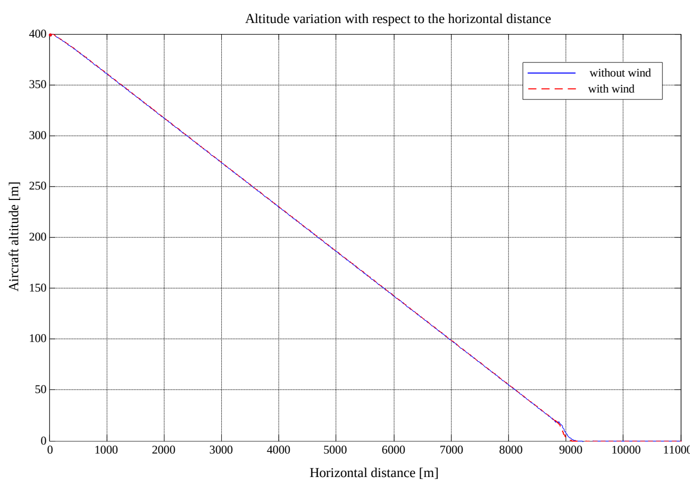

Fig. 27 The landing trajectories $H = H(x)$ for the ALS based on the dynamic inversion concept

VII. Conclusions

The automatic landing systems have subsystems for the control of the aircraft longitudinal velocity, control laws based on the dynamic inversion principle, slope controllers, flare controllers, conventional PD and PID controllers or PD and PID fuzzy controllers. The disturbances, which are taken into account in this paper, are the longitudinal and the vertical wind shears. Two types of ALS were developed and validated through numerical simulations: 1) ALS with ILS system; and 2) ALS which controls the altitude by means of the state vector.

For the ALS with ILS system the wind shears insignificantly affect the transient regime of the two landing phases – the differences between the solid curves and the dashed ones are minor; the steady regime is not affected (the steady values of the variables are the same). The trajectories $H(t)$ are less influenced by the wind shears. The transient regime period is approximately the same for the two cases (with or without taking into consideration the wind shears). For the second ALS, which controls the altitude by means of the state vector (ALS based on dynamic inversion, using conventional controllers), the wind shears affect insignificantly the two landing phases – the amplitudes of the signals are approximately the same for the glide slope landing phase and flare phase. The transient regime period is approximately the same for the two cases (with or without taking into consideration the wind shears). From the system transient regime period and overshoot point of view, the ALS based on dynamic inversion works better than the ALS with ILS system and conventional controllers. However, a significant improvement of the performance was obtained by replacing the conventional controllers with fuzzy controllers in the ALS with ILS system. More than that, the performances of the intelligent controlled ALS with ILS system are better than in the case of the ALS based on dynamic inversion. The numerical simulations show also the superiority of the dynamic qualities for the ALS with fuzzy controllers, especially in the case of strong wind shears.

The authors also take into consideration the errors of the sensors for the measurement of system variables. It was observed that the sensor errors produce an increase of the signals amplitude in the transient regime and very small oscillations in the steady regime, but these errors do not affect the two landing phases.

The authors' contributions in this paper may be evidenced by the analysis of the two command systems. Thus, for the ALS in Fig. 3 and the system model in Fig. 5 the following original issues can be mentioned:

1) the model of the ILS subsystem takes into consideration the time variation of the variable $R = R(t)$, compared with Donald's paper (Donald 1990), where the aproximation $R = R_0 = R(0)$ is made;
2) unlike other systems, our automatic landing systems have a low – pass filter, after the ILS, and a high – pass filter on the direct way of the controller for the pitch angle θ;
3) the design of the altitude controller for the glide slope phase and flare phase, both in classical and fuzzy logic approaches;
4) the design of the pitch angle controller (PD conventional controller and PD fuzzy logic controller);
5) the design of the longitudinal velocity controller, having as subsystem a first order command filter; the order is equal with the relative degree with respect to the variable V_x ;
6) the control laws of the three controllers (conventional or fuzzy) are chosen so that the system is easily configurable: the signals provided by the transducers for the velocity V_x and pitch angle θ must be replaced by a strap – down navigation system (consisting of accelerometers and gyros); the velocity V_x is obtained by the integration of the signal provided by the accelerometer a_x (placed along the longitudinal axis of the aircraft), while the pitch angle is obtained by the integration of the signal provided by the pitch angular rate gyro (ω_y); this signal, together with the one provided by an attack angle sensor (or an overload sensor), are used for the calculus of the flight path angle $\gamma = \theta - \alpha$, of the descend velocity $\dot{H}$, and of the altitude H

(without the usage of an altimeter); so, only three sensors are necessary (a sensor for the acceleration a_x, a sensor for the attack angle α, and a sensor for the pitch angular rate ω_y);

7) the study of the errors induced by the longitudinal and vertical wind shears and by the gyro errors, using conventional or fuzzy controllers.

For the ALS in Fig. 4 the following original issues can be mentioned:

1) the geometry of the landing process (the model for the calculus of the variables $x_{p_o}, \tau, x, \dot{x}, H_c$);
2) the design of the PID controller for the altitude H (equation (32)), the design of the command filter (reference model) for the pitch angle – equation (31), the design of the PID controller for the pitch angle (equation (30)), and the synthesis of the control law δ_{p_c} by using the dynamic inversion concept (equation (26));
3) the design of the PID controller for the velocity V_x (equation (33)), the synthesis of the control law δ_{T_c} by using the dynamic inversion concept (equation (27)), and the design of the afferent command filter;
4) the same with the ones presented above (ALS with ILS) to the points 6) and 7).

Acknowledgments

This work was supported by CNCSIS-UEFISCSU, project PN II-RU, No. 1/28.07.2010, “High-precision strap-down inertial navigators, based on the connection and adaptive integration of the nano and micro inertial sensors in low cost networks, with a high degree of redundance”, code TE_102/2010. Also, all the three authors had equal contributions to this work preparation.

References

[1] Donald, Mc. L. (1990).” Automatic Flight Control Systems”, *Prentice Hall Publisher*.

[2] Aron, I., Lungu, R., and Cismaru, C. (1989).” Sisteme de navigatie aerospatiala”, *Scrisul Romanesc Publisher*, Craiova.

[3] Singh, S., and Padhi, R. (2008). “Automatic Landing of Unmanned Aerial Vehicles Using Dynamic Inversion,” *Proceedings of the International Conference on Aerospace Science and Technology,* 26 – 28 June, Bangalore, India.

[4] Juang, J. G., and Cheng, K. C. (2006). “Application of Neural Network to Disturbances Encountered Landing Control,” *IEEE Transactions on Intelligent Transportation Systems*, vol.7, no.4, pp. 582 – 588.

[5] Lungu, M. (2008). “Sisteme de conducere a zborului”, *Sitech Publisher*.

[6] Che, J., and Chen, D. (2001). “Automatic Landing Control using H_∞ control and Stable Inversion,” *Proceedings of the 40th Conference on Decision and Control*, Orlando, Florida, USA, pp. 241 – 246.

[7] Kang, W., and Isidori, A. (1992). “Flight Control in a Windshear via Nonlinear H_∞ Methods,” *Proceedings of the 31st Conference on Decision and Control*, pp. 1135 – 1142.

[8] Kawaguchi, J. I., Miyazawa, Y., and Ninomiya, T. (2008). “Flight Control Law Design with Hierarchy – Structured Dynamic Inversion Approach,” *AIAA Guidance, Navigation and Control Conference Exhibit*.

[9] Calise, A. J., and Rysdyk, R. T. (1999). “Adaptive Model Inversion Flight Control for Tiltrotor Aircraft,” *AIAA Guidance, Navigation and Control*, vol. 22, pp. 402 – 407.

[10]Pashilkar, A. A., Sundararajan, N., and Saratchhandran, P. A. (2006). “Fault-Tolerant Neural Aided controller for Aircraft Auto-Landing,” *Aerospace Science and Technology* , vol. 10. Issue 1, pp. 49 – 61.

[11]Lungu, R. (2000). “Automatizarea aparatelor de zbor”, *Universitaria Publisher*, Craiova.

[12]Lungu, R. (1997). “Echipamente si sisteme giroscopice”, *Universitaria Publisher*, Craiova.

[13]Aron, I., and Lungu, R. (1994). “Automatica girostabilizatoarelor”, *Enciclopedica Publisher*, Bucharest.

[14]Lungu, R., and Grigorie, L. (2005).” Traductoare accelerometrice si girometrice”, *Sitech Publisher*, Craiova.

[15]Grigorie, T. L. (2007). ”Strap-down inertial navigation systems. Optimization studies”, *Sitech Publisher*, Craiova.

[16]Federal Aviation Administration (1971). “Automatic Landing Systems”. AC 20 – 57 A.

[17]Niewoenhner, R. J., and Kaminer, I. I. (1996). “Design of an Autoland Controller for an F-14 Aircraft Using H_∞ Synthesis,” *Journal of Guidance, Control and Dynamics*, vol. 19, no. 3, pp. 656 – 663.

[18]Liao, F., Wang, J. L., and Poh, E. K. (2005). “Fault – Tolerant Robust Automatic Landing Control Design,” *Journal of Guidance, Control and Dynamics*, vol. 28, no. 5, pp. 854 – 871.

[19]Mori, R., and Suzuki, S. (2009). “Neural Network Modeling of Lateral Pilot Landing Control,” *Journal of Aircraft*, no. 46, pp. 1721 – 1726.

[20]Niculescu, M. (2001). “Lateral Track control Law for Aerosonde UAV,” *AIAA 2001 – 0016*, pp. 1 – 11.

[21]MIT Open Course Ware Web site (2007). “Aircraft Lateral Autopilots”.

[22]Kargin, V. (2007). “Design of An Autonomous Landing Control Algorithm for A fixed Wing UAV” M.S. Thesis, Middle East Technical University, Ankara, Turkey.

[23]Vo, H., and Sridhar, S. (2008). “Robust Control of F-16 Lateral Dynamics,” *International Journal of Aerospace and Mechanical Engineering*, pp. 80 – 85.

[24]Abdullah I. A., and Ayman, A. A. (2008). ”The Advantages of PID Fuzzy Controllers Over The Conventional Types,” *American Journal of Applied Sciences*, 5 (6), pp. 653-658.

[25]Zdenko K., and Stjepan B. (2006). “Fuzzy Controller Design – Theory and applications”, *Taylor and Francis Group*.

[26]Verbruggen, H. B., and Bruijn, P. M. (1997). “Fuzzy control and conventional control: What is (and can be) the real contribution of Fuzzy Systems?” *Fuzzy Sets Systems*, Volume 90 , Issue 2, pp. 151–160.

[27]Hampel, R., Wagenknecht, M., and Chaker, N. (2000). ” Fuzzy Control – Theory and Practice”, *Physica-Verlag Publisher*.

[28]Zadeh, L. A. (1965). “Fuzzy sets”, *Information Control Journal*, Vol. 8, pp. 339-353.

[29]Tomescu, B. (2001). “On the use of fuzzy logic to control paralleled dc-dc converters”. Dissertation - Virginia Polytechnic Institute and State University Blacksburg, Virginia, October.

[30]Jantzen, J. (1998). ”Tuning of fuzzy PID controllers”. Technical Report 98-H871, Department of Automation, Technical University of Denmark.

[31]Kumar, V., Rana, K. P., and Gupta, V. (2008). “Real-Time Performance Evaluation of a Fuzzy PI + Fuzzy PD Controller for Liquid-Level Process,” *International Journal of Intelligent Control and Systems*, Vol. 13, No. 2, pp. 89-96.

[32]Mahfouf, M., Linkens, D. A., and Kandiah, S. (1999). “Fuzzy Takagi-Sugeno Kang model predictive control for process engineering”, *IEE Savoy Place Publisher*, London, WCPR OBL. UK.